Supplement of

Bulk and Molecular-Level Characterization of Laboratory-Aged Biomass Burning Organic Aerosol from Oak Leaf and Heartwood Fuels

Claire F. Fortenberry, et al.

Correspondence to: Brent J. Williams (brentw@wustl.edu)
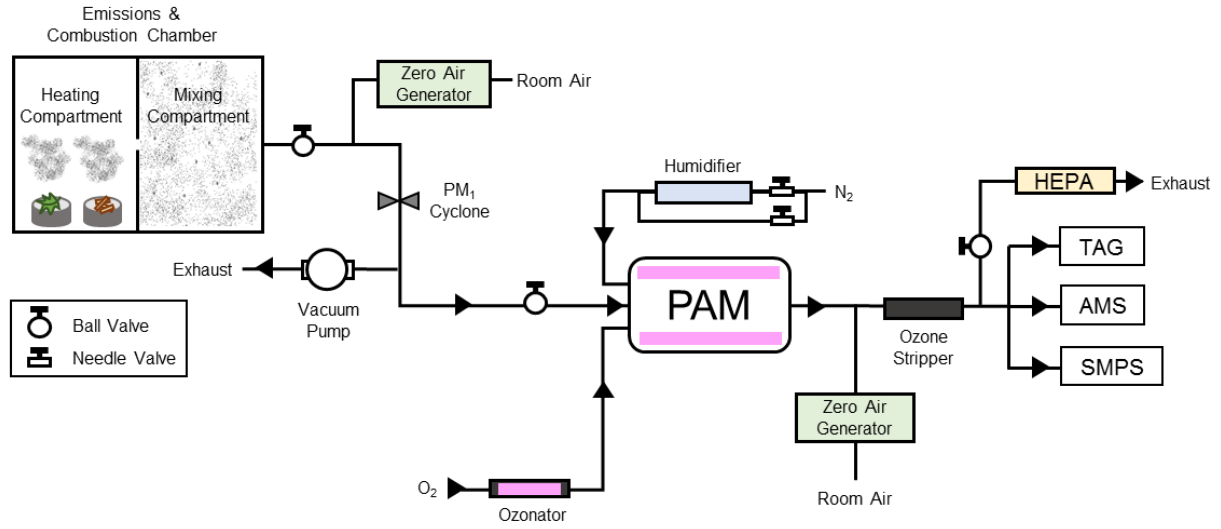
Figure S1: Flow diagram of experimental setup
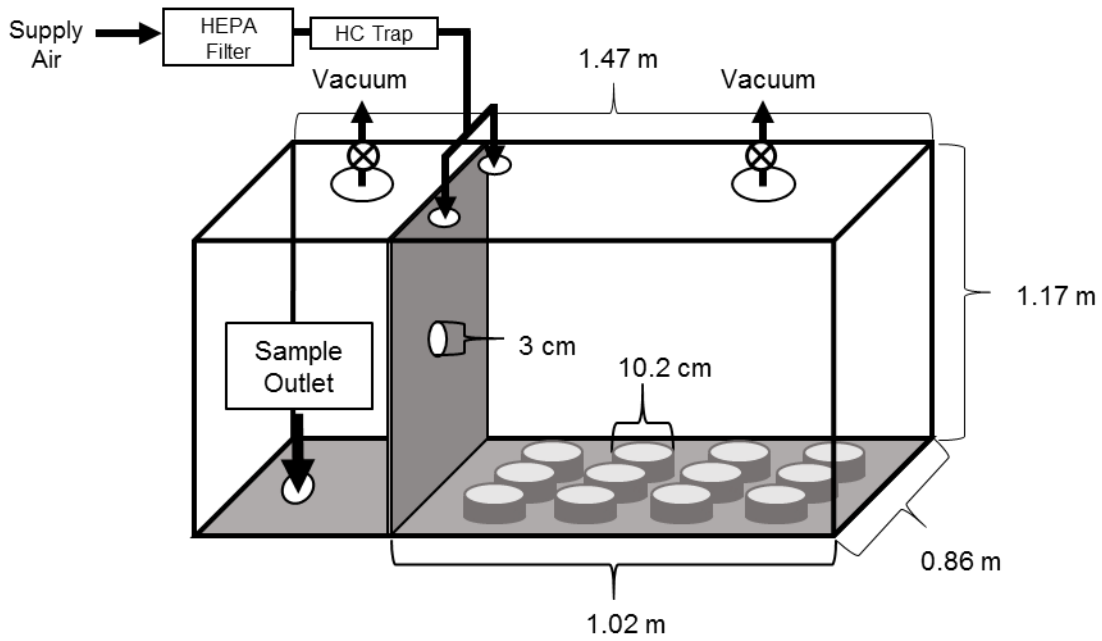
Figure S2: Diagram of emissions and combustion chamber.

Method: PAM Calibrations

The PAM was calibrated a week prior to the first experimentation period. Equivalent atmospheric aging times were determined by calibrating the PAM reactor with sulfur dioxide (SO_2) gas, as described by Kang, et al (Kang et al., 2007). A constant stream of SO_2 (Airgas, Inc., Radnor, PA) was introduced into the PAM chamber at a steady flow rate of 0.02 L min^{-1}. Humidified N_2 (RH = 30%) and O_2 flow rates were maintained at 4.6 L min^{-1} and 0.4 L min^{-1}, respectively. The total flow rate through the PAM chamber was maintained at 10 L min^{-1} throughout the calibration. The PAM ultraviolet (UV) lamp voltage was systematically varied from 30 to 100V, and the SO_2 concentration was measured for 25 minutes at each setting using an SO_2 analyzer (Model 43i-TLE, Thermo Fischer Scientific, Waltham, MA). OH· exposure (OH_{exp}), defined as the OH· concentration multiplied by the reactor residence time, was calculated based on a pseudo-first order rate expression for the reaction of SO_2 with OH·:

$$\frac{d[SO_2]}{dt} = -k_{OH}[OH][SO_2]$$

$$OH_{exp} = [OH]t = \frac{1}{k_{OH}} ln\left(\frac{[SO_2]_0}{[SO_2]}\right)$$

where k_{OH} is the rate constant for the reaction of SO_2 with OH· (9×10^{-13} cm^3 molec^{-1} s^{-1} ; Davis et al., 1979; Lambe et al., 2011) and $[SO_2]_0$ is the initial SO_2 concentration.

Equivalent aging times (t_{equiv}) were determined for each voltage setting assuming an average atmospheric OH· concentration ($[OH]_{atm}$) of 1.5×10^6 molec cm^{-3} (Mao et al., 2009) and a reactor residence time of 78 seconds:

$$t_{equiv} = \frac{[OH]_{atm}}{OH_{exp}}$$

To obtain OH_{exp} and equivalent aging times for each PAM UV lamp setting, the results of the calibration were fit with a linear regression ($r^2 = 0.957$). OH_{exp} and equivalent aging time values are given as functions of the PAM light voltage in Figure S3a.

OH· forms in the PAM reactor when monatomic oxygen radicals, produced as a result of O_3 UV (254 nm) photolysis, react with water molecules (Ehhalt et al., 1990; Lambe et al., 2011; Levy, 1971; Palm et al., 2016; Shetter et al., 1996). Previous PAM studies have demonstrated that OH· production increases with increasing relative humidity (RH) (Kang et al., 2007; Li et al., 2015; Peng et al., 2015, 2016). The sensitivity of OH_{exp} to RH in our PAM reactor was investigated by performing SO_2 calibrations at 10%, 20%, and 30% RH (Figure S3b).
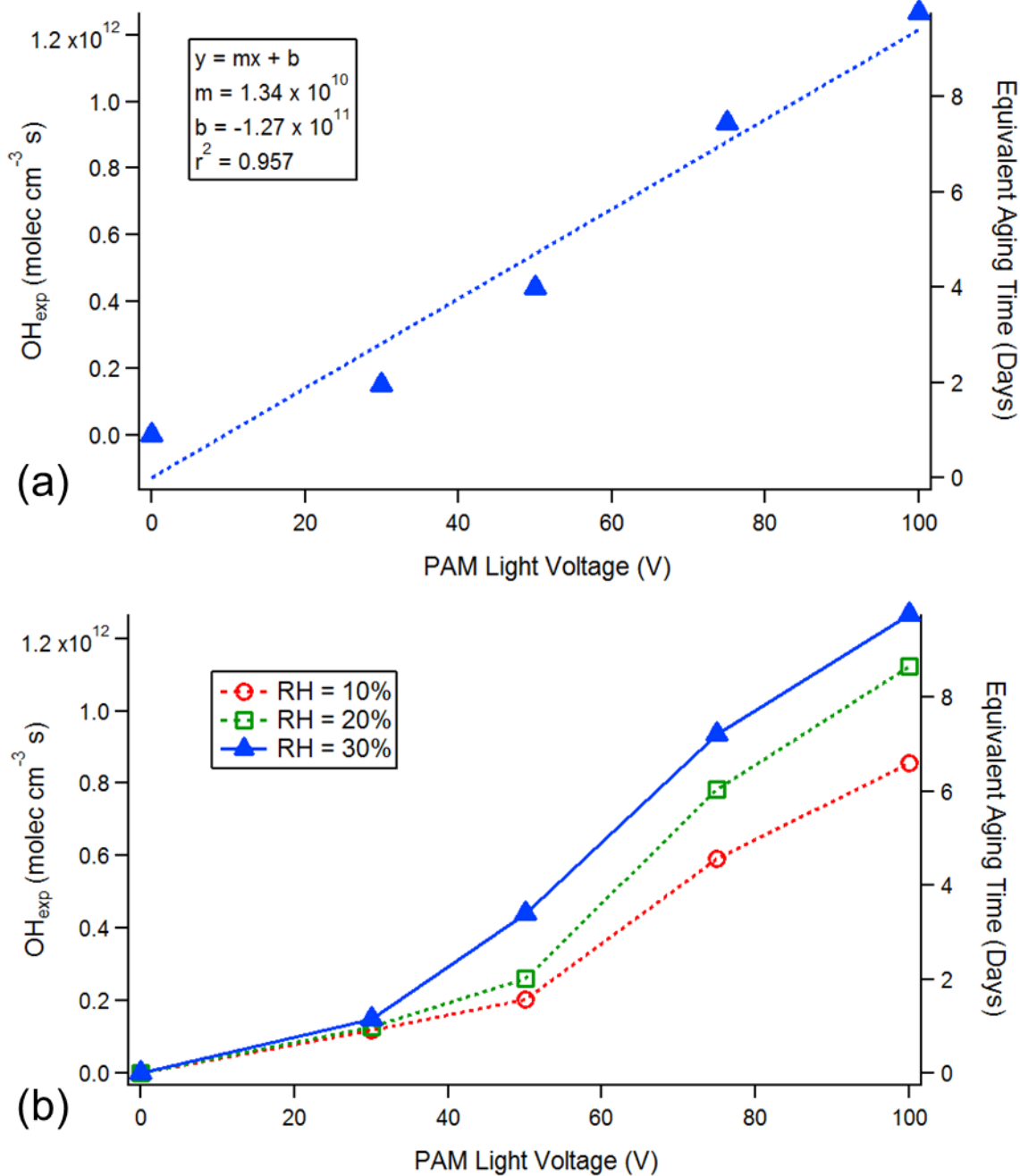
Figure S3. Results from PAM reactor SO_2 calibrations, displayed as OH_{exp} and equivalent aging times as functions of PAM reactor light voltage. **(a)** results from the calibration at RH = 30%, with linear regression parameters provided; **(b)** results from calibrations at 10% (red circles), 20% (green squares), and 30% (blue triangles) RH.
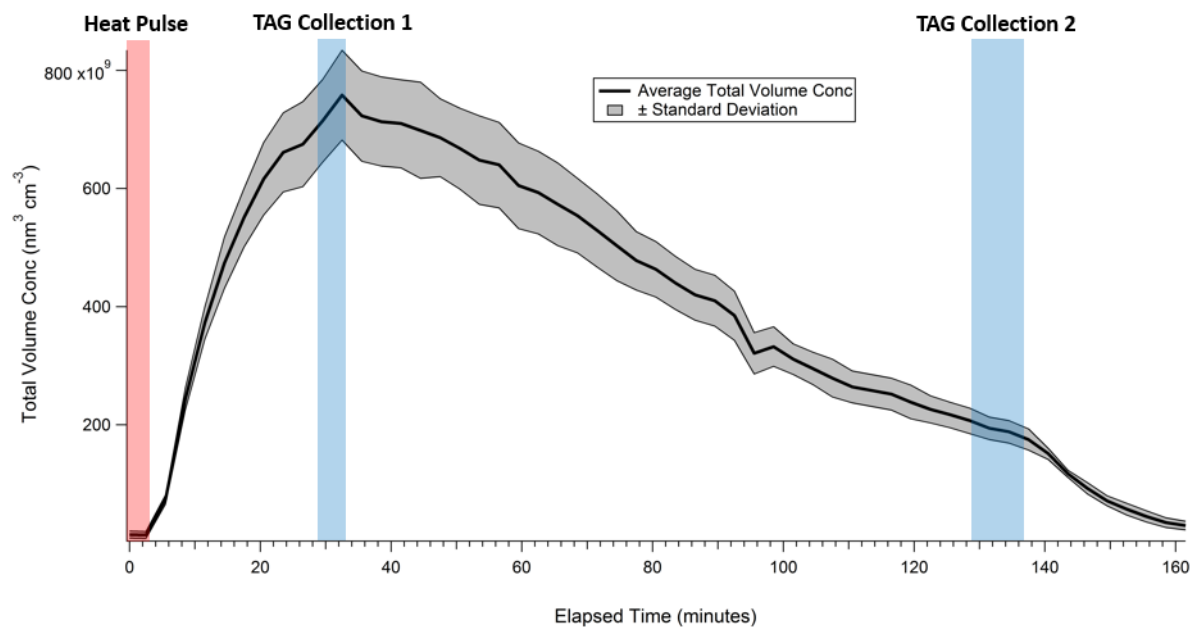
Figure S4. SMPS total volume concentration (nm^3 cm^{-3}) over time for oak heartwood PM_1 at 3.4 days of equivalent aging, presented as an average of triplicate measurements (bold black trace) ± one standard deviation (gray shaded region). The heat pulse occurred during the period encompassed by the red shaded region, beginning at elapsed time = 0 minutes. All TAG data presented in this work were collected for a duration of 4 minutes beginning 30 minutes after the start of the heat pulse (blue shaded region, "TAG Collection 1"). Additional sample collections (e.g. blue shaded region, "TAG Collection 2"; other subsequent collections not shown) were also obtained to evaluate the cleanliness of the emissions and combustion chamber.
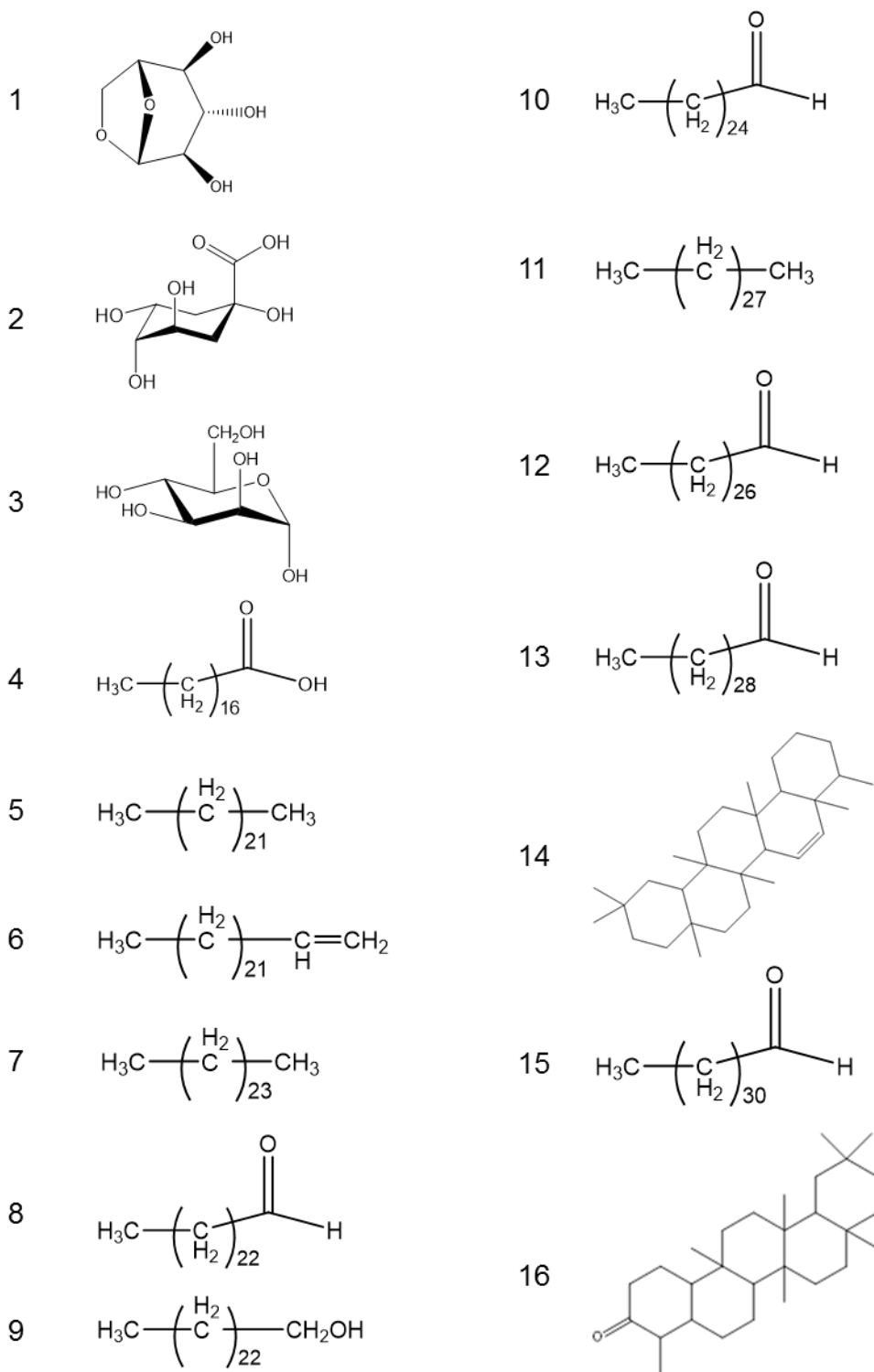
Figure S5: Structures identified in oak leaf BBOA TAG chromatograms. Corresponding compound names are provided in Table S2.
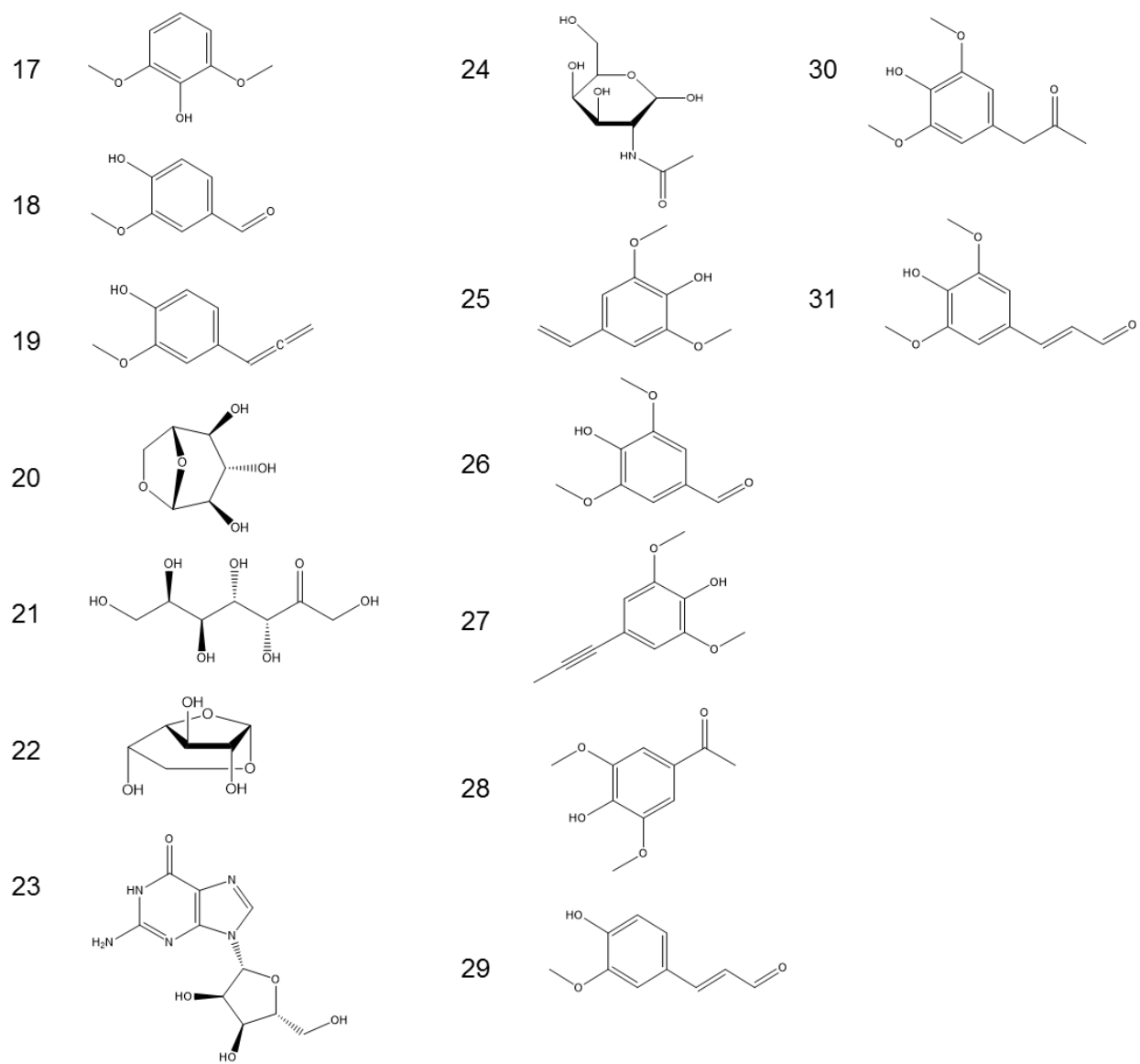
Figure S6: Structures identified in oak wood BBOA TAG chromatograms. Corresponding compound names are provided in Table S3.

Method: Oak leaf solvent extractions

The solvent extraction method used to extract leaf wax components was adapted from a previously published method (Gulz and Boor, 1992). A 52.9 ± 0.5 mg leaf sample was gently broken into roughly centimeter-wide pieces and added to 2 mL of a 2:1:1 mixture of chloroform, acetone, and methanol. The leaf sample was submerged in the solvent mixture for one minute under gentle agitation by hand. The leaf was then removed for one minute and submerged again for one minute. Solid leaf components were decanted from the extraction prior to TAG analysis. A 3 µL aliquot of the extraction was injected onto the TAG CTD cell through its standard injection port (Kreisberg et al., 2009), desorbed, separated, and analyzed using the previously described TAG thermal desorption and GC oven programs.
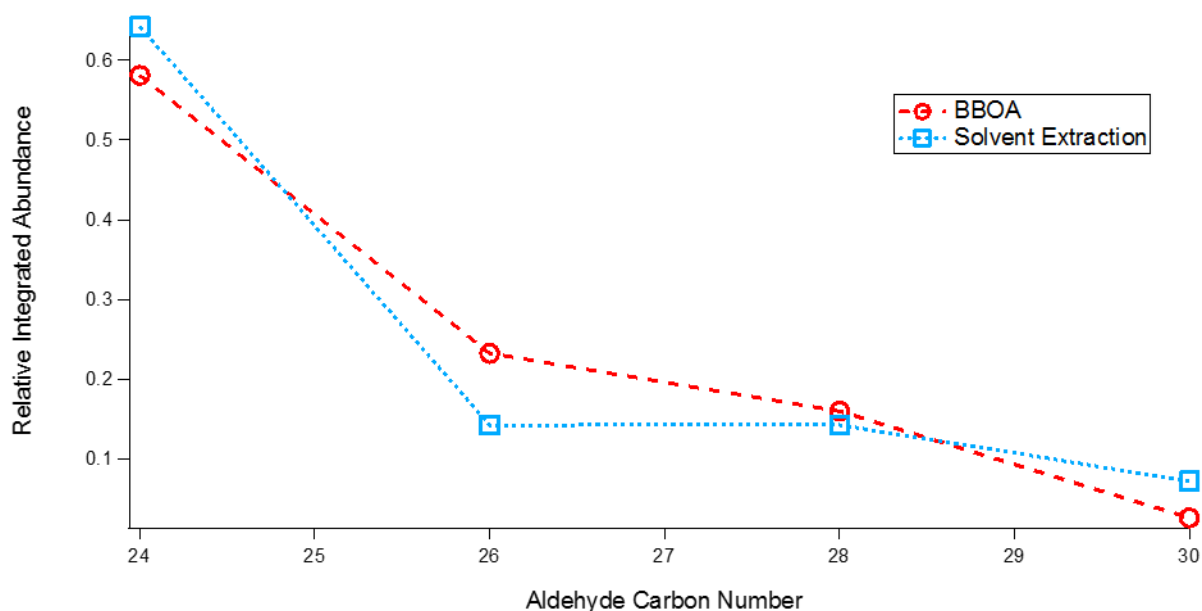
Figure S7. Relative integrated abundances for four different aldehydes measured in a TAG leaf BBOA chromatogram (0 days of equivalent aging) and a solvent extraction chromatogram. Each point corresponds to the integrated *m/z* 82 abundance normalized to the sum of the integrated *m/z* 82 abundances over the four different aldehydes within the chromatogram.
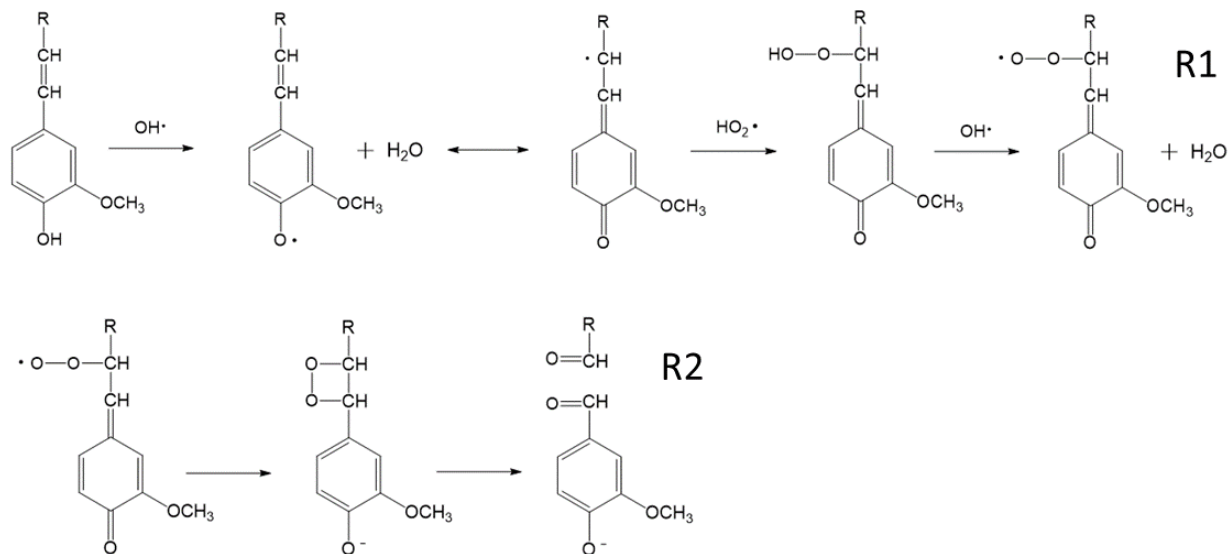
Figure S8. One possible mechanism for the formation of vanillin from larger lignin decomposition products within the PAM reactor. In the first stage (**R1**), a peroxy radical intermediate is formed following OH·-driven hydrogen abstraction from the phenolic substituent, rearrangement, and HO_2 radical addition to the beta carbon. In the second stage (**R2**), the radical intermediate undergoes an intramolecular nucleophilic attack, causing breakage of the C_α-C_β bond and resulting in formation of two distinct aldehydes. This mechanism assumes sufficiently high concentrations of the HO_2 radical are present within the reactor. The mechanism was adapted from the alkaline oxygen delignification mechanism described by Wong, et al. (Wong et al., 2010).
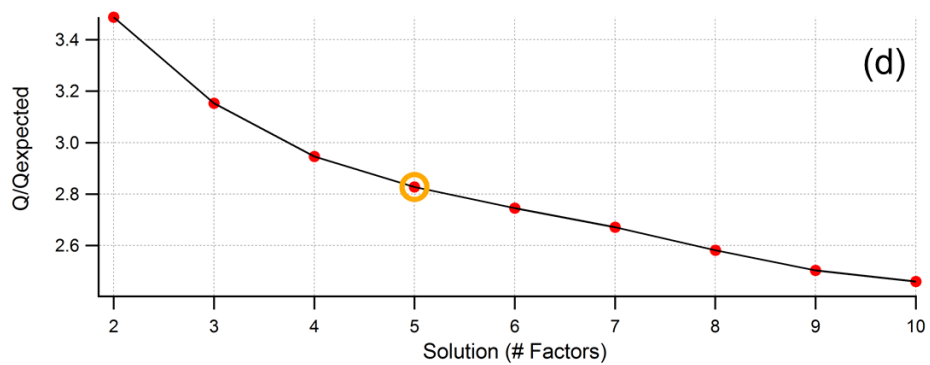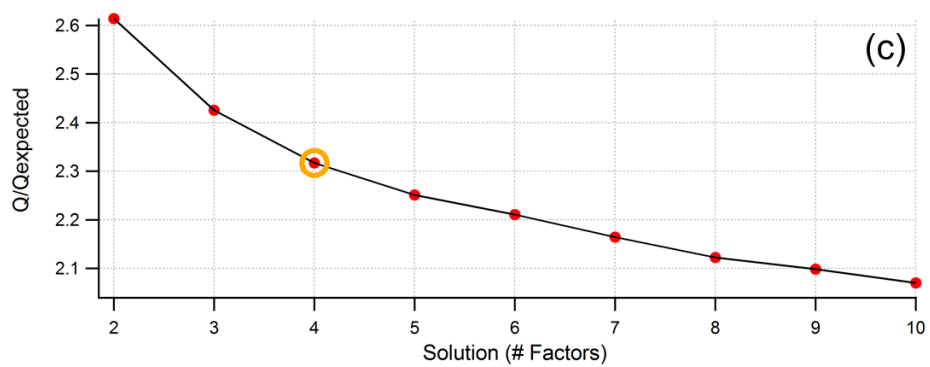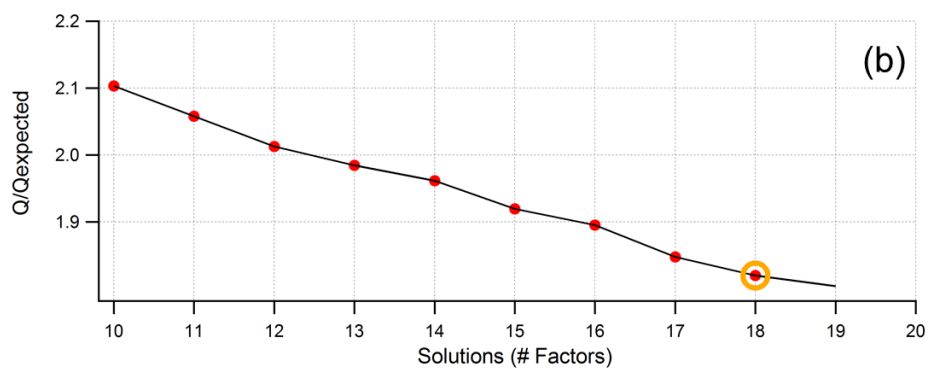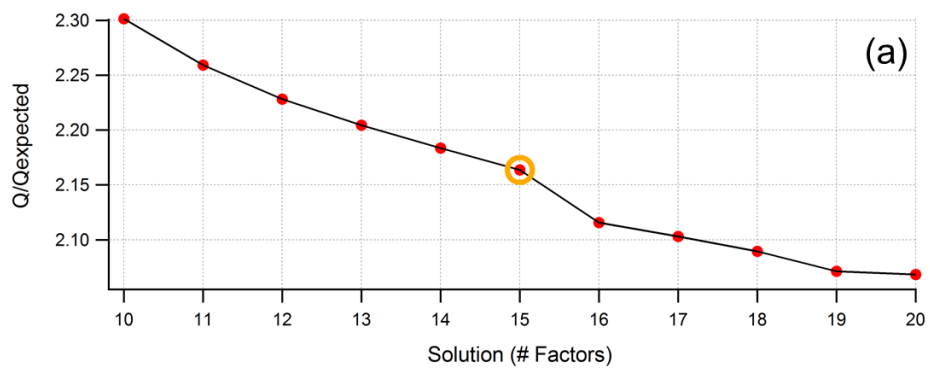
Figure S9. Q/Q_{exp} as a function of factor number, where the orange circle indicates the number of factors in the chosen solution for PMF calculations on: **(a)** oak leaf compound window; **(b)** oak wood compound window; **(c)** oak leaf decomposition window; **(d)** oak wood decomposition window.
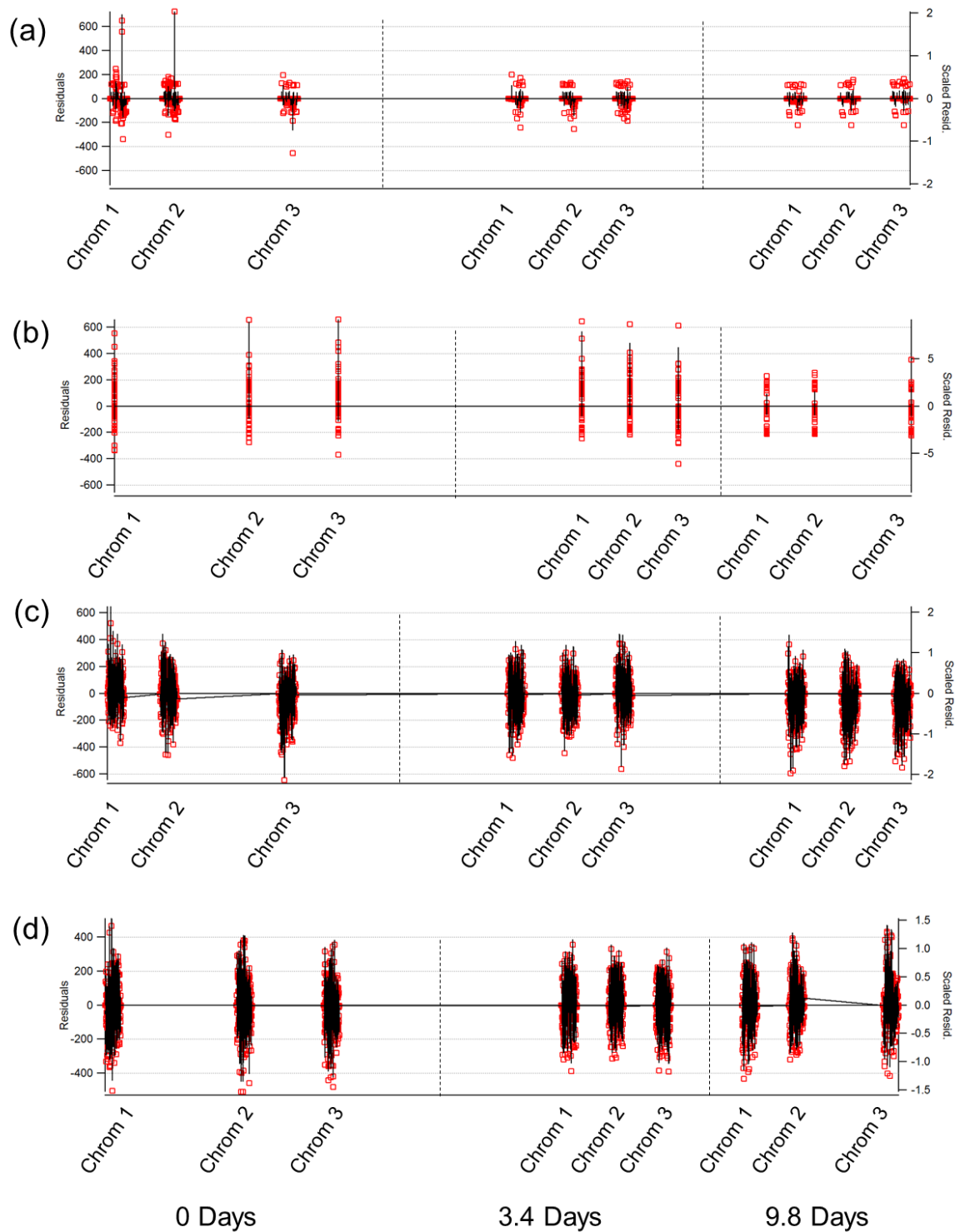
Figure S10. Residuals (black lines) and scaled residuals (red dots) from PMF calculations on: **(a)** oak leaf compound window; **(b)** oak wood compound window; **(c)** oak leaf decomposition window; **(d)** oak wood decomposition window.
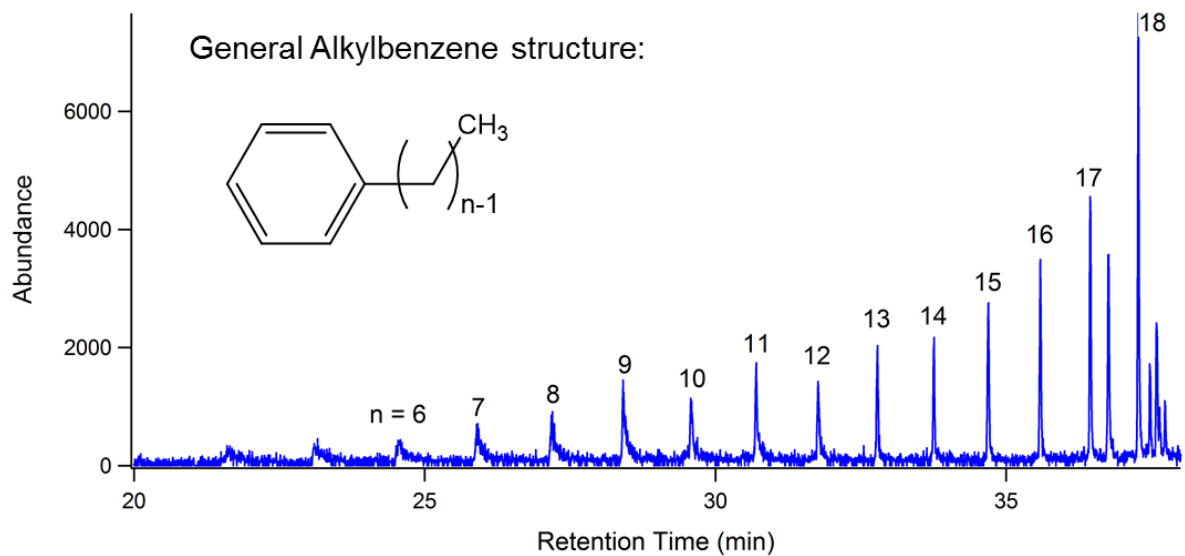
Figure S11. *m/z* 92 single ion chromatogram (SIC) from TAG analysis of oak leaf extract showing a series of alkylbenzenes. The number above each peak denotes the number of carbons (*n*) present in the alkyl chain (e.g. *n* = 9 corresponds to nonyl-benzene).
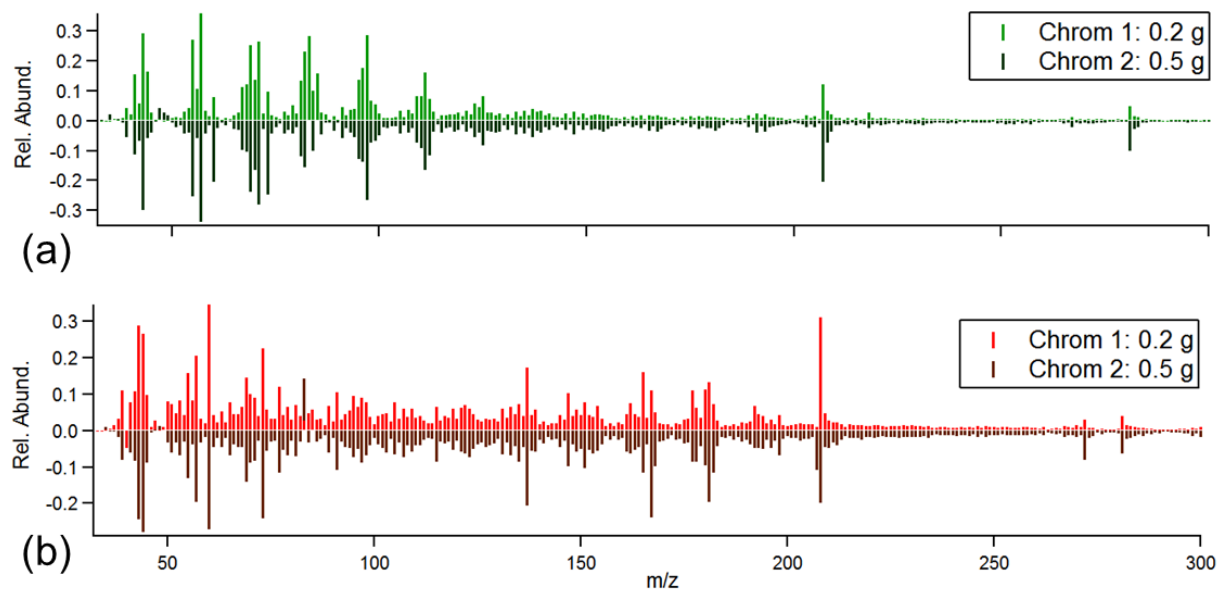
Figure S12. Summed mass spectra for unaged BBOA chromatograms obtained using 0.2 g ("Chrom 1") and 0.5 g ("Chrom 2") of: **(a)** oak leaf, and **(b)** oak wood. Each mass spectrum was obtained from the chromatogram by subtracting an appropriate system blank, summing all ions across the full chromatogram, and converting the resulting mass spectrum vector to a unit vector per the technique outlined in Stein and Scott (Stein and Scott, 1994). In both plots, the "Chrom 2" unit vector is displayed with a negative relative abundance to facilitate visual comparison of the mass spectra.
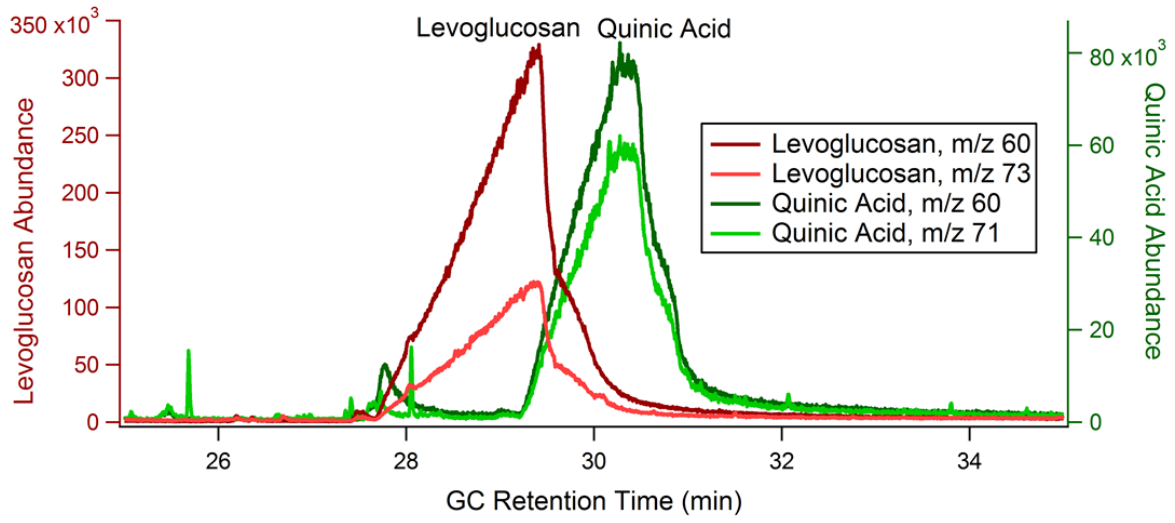
Figure S13. Results from levoglucosan (15 μg) and quinic acid (5 μg) TAG standard injections.
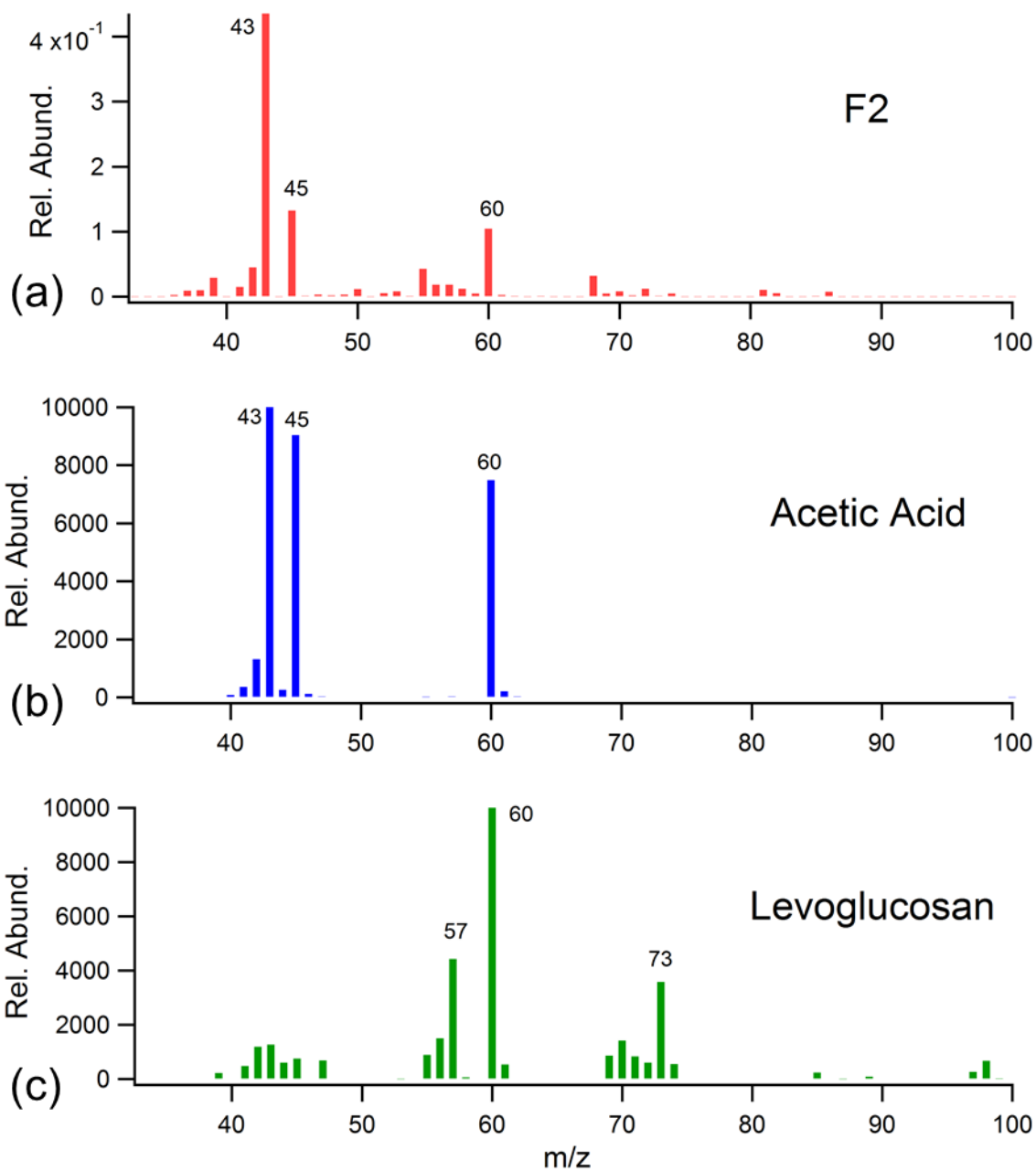
Figure S14. Electron ionization mass spectra for **(a)** Factor 2 (F2) obtained during oak wood decomposition PMF analysis (Figure 13), **(b)** Acetic acid (NIST Mass Spec Data Center), and **(c)** levoglucosan (NIST Mass Spec Data Center).

Table S1. OH_{exp} estimations obtained using the Oxidation Flow Reactor Exposure Estimator version 2.3, available for download at http://sites.google.com/site/pamwiki/hardware/estimation-equations (Peng et al., 2015). Calculations were performed using the OFR185 portion of the spreadsheet. For low and high (1 and 100 s^{-1}, respectively) assumed external OH reactivity (OHR_{ext}) values, OH_{exp} was calculated output using O_3 concentrations typical of each level of oxidation ([O_3]; obtained during reactor calibrations), a reactor residence time of 78 s, and an RH of 30%. The cells of the table are color-coded to indicate whether the "condition type" was determined to be "safer" (green) or "riskier" (orange).

Qualitative Level of Oxidation[a]	Equiv. Aging Time (days)[a]	[O_3] (ppm)	OH_{exp} (molec cm^{-3} s)	
			$OHR_{ext} = 1$ s^{-1}	$OHR_{ext} = 100$ s^{-1}
Low-mid	3.4	4.3	2.5×10^{12}	3.5×10^{11}
High	9.8	8.5	5.3×10^{12}	1.0×10^{12}

[a] See Table 1.

Table S2. Maximum SMPS volume concentrations (μm^3 cm^{-3}) at each level of oxidative aging, presented as an average of triplicate measurements ± one standard deviation.

Fuel Type	Equivalent Aging Time (days)		
	0	3.4	9.8
Leaf	314.20 ± 78.59	210.97 ± 40.82	179.04 ± 28.44
Wood	606.52 ± 45.32	813.73 ± 5.61	791.48 ± 37.61

Table S3. Selected compounds of interest identified in oak leaf BBOA TAG chromatograms. Common compound names were used in this work where appropriate and are provided in parentheses. Estimated subcooled liquid vapor pressures (p_L°), saturation concentrations (C^*) and corresponding volatility classifications are also provided. Compounds are classified as intermediately volatile, semivolatile, low volatility, or extremely low volatility organic compounds (I-, S-, L-, ELVOCs, respectively) based on the compound's $\log_{10}(C^*)$ value and criteria outlined in previous literature.

Structure	Compound Name	Certainty of ID[a]	Molecular Formula	Predicted p_L° at 25°C (torr)[b]	$\log_{10}(C^*)$ ($\mu g\ m^{-3}$)[c]	Volatility Classification[d]
1	1,6-anhydro-β-glucopyranose (levoglucosan)	A	$C_6H_{10}O_5$	1.81E-7	0.31	SVOC
2	Quinic Acid	A	$C_7H_{12}O_6$	1.58E-9	-1.67	LVOC
3	Mannose	B	$C_{16}H_{12}O_6$	2.59E-13	-5.49	ELVOC
4	Octadecanoic Acid	B	$C_{18}H_{36}O_2$	8.58E-6	2.23	SVOC
5	Tricosane (C_{23} alkane)	A	$C_{23}H_{48}$	1.24E-05	2.45	SVOC
6	Tetracosene (C_{24} alkene)	D	$C_{24}H_{48}$	8.07E-06	2.28	SVOC
7	Pentacosane (C_{25} alkane)	A	$C_{25}H_{52}$	5.90E-06	1.82	SVOC
8	Tetracosanal (C_{24} aldehyde)	D	$C_{24}H_{48}O$	7.34E-08	2.16	SVOC
9	Tetracosanol (C_{24} alcohol)	D	$C_{24}H_{50}O$	1.85E-06	0.260	SVOC
10	Hexacosanal (C_{26} aldehyde)	D	$C_{26}H_{52}O$	1.47E-07	1.69	SVOC
11	Nonacosane (C_{29} alkane)	A	$C_{29}H_{60}$	6.18E-07	0.623	SVOC
12	Octacosanal (C_{28} aldehyde)	D	$C_{28}H_{56}O$	2.19E-07	1.25	SVOC
13	Triacontanal (C_{30} aldehyde)	D	$C_{30}H_{60}O$	8.22E-08	0.825	SVOC
14	D:A-Friedoolean-6-ene	B	$C_{30}H_{50}$	6.15E-08	0.247	SVOC
15	Dotriacontanal (C_{32} aldehyde)	D	$C_{32}H_{64}O$	2.86E-09	0.426	LVOC
16	Friedelan-3-one (Friedelin)	B	$C_{30}H_{50}O$	1.24E-05	-1.07	LVOC

[a] Identification certainty ("Certainty of ID") was classified for each compound according to the following criteria: (A) the compound was positively identified based on external standard injections; (B) the compound was identified based on a high match quality (MQ > 75%) using available mass spectral libraries; (C) the compound was identified based on a low-to-moderate match quality (MQ < 75%) using available mass spectral libraries; and (D) no adequate mass spectral library match was available for the compound, so the compound structure was determined by retention time and manually evaluating possible fragmentation patterns.
[b] Vapor pressures at 25°C were predicted using the Advanced Chemistry Development (ACD/Labs) Software V11.02 (© 1994-2017 ACD/Labs) through the SciFinder website (ACD/Labs, 2017).
[c] $\log_{10}(C^*)$ values calculated using methods outlined in Pankow, et al. (Pankow, 1994). An activity coefficient of 1.3 was assumed based on a typical estimated BBOA activity coefficient of 1.3 (Donahue et al., 2011).
[d] Defined using criteria set forth in previous work (Donahue et al., 2011, 2012).

Table S4. Selected compounds of interest identified in oak wood BBOA TAG chromatograms. Common compound names were used in this work where appropriate and are provided in parentheses. Estimated subcooled liquid vapor pressures (p_L°), saturation concentrations (C*) and corresponding volatility classifications are also provided. Compounds are classified as intermediately volatile, semivolatile, low volatility, or extremely low volatility organic compounds (I-, S-, L-, ELVOCs, respectively) based on the compound's $\log_{10}$(C*) value and criteria outlined in previous literature.

Structure	Compound Name	Certainty of ID[a]	Molecular Formula	Predicted $p_L^{\circ b}$	$\log_{10}$(C*) ($\mu g\ m^{-3}$)[c]	Volatility Classification[d]
17	2,6-dimethoxy-phenol (syringol)	B	$C_8H_{10}O_3$	5.91E-3	4.80	IVOC
18	4-hydroxy-3-methoxy-benzaldehyde (vanillin)	B	$C_8H_8O_3$	1.94E-3	4.31	IVOC
19	4-(1,2-propadienyl)-guaiacol	B	$C_{10}H_{10}O_2$	1.16E-3	4.12	IVOC
20	1,6-anhydro-β-glucopyranose (levoglucosan)	A	$C_6H_{10}O_5$	1.81E-7	0.31	SVOC
21	galacto-heptulose	C	$C_7H_{14}O_7$	2.08E-18	-10.51	ELVOC
22	1,6-anhydro-α-d-galactofuranose	C	$C_6H_{10}O_5$	1.12E-8	-0.896	LVOC
23	guanosine	C	$C_{10}H_{13}N_5O_5$	2.44E-25	-17.32	ELVOC
24	n-acetyl-d-galactosamine	C	$C_8H_{15}NO_6$	7.12E-9	-10.96	ELVOC
25	2,6-di-methoxy-4-vinyl-phenol (4-vinyl-syringol)	B	$C_{10}H_{12}O_3$	1.63E-3	4.31	IVOC
26	4-hydroxy-3,5-dimethoxy-benzaldehyde (syringaldehyde)	B	$C_9H_{10}O_4$	1.51E-4	3.28	IVOC
27	2,6-dimethoxy-4-(1-propynyl)-phenol	C	$C_{11}H_{12}O_3$	8.95E-5	3.08	IVOC
28	1-(4-hydroxy-3,5-dimethoxyphenyl)-ethanone (acetosyringone)	B	$C_{10}H_{12}O_4$	6.49E-5	2.95	IVOC
29	3-(4-hydroxy-3-methoxyphenyl)prop-2-enal (coniferaldehyde)	B	$C_{10}H_{10}O_3$	4.88E-5	2.78	IVOC
30	4-(2-oxopropyl)-syringol (syringyl acetone)	B	$C_{11}H_{14}O_4$	4.49E-5	2.82	IVOC
31	4-hydroxy-3,5-dimethoxycinnamaldehyde (sinapaldehyde)	B	$C_{11}H_{12}O_4$	4.53E-6	1.82	SVOC

[a] Identification certainty ("Certainty of ID") was classified for each compound according to the following criteria: (A) the compound was positively identified based on external standard injections; (B) the compound was identified based on a high match quality (MQ > 75%) using available mass spectral libraries; (C) the compound was identified based on a low-to-moderate match quality (50% < MQ < 75%) using available mass spectral libraries; and (D) no adequate mass spectral library match was available for the compound, so the compound structure was determined by retention time and manually evaluating possible fragmentation patterns.

[b] Vapor pressures at 25°C were predicted using the Advanced Chemistry Development (ACD/Labs) Software V11.02 (© 1994-2017 ACD/Labs) through the SciFinder website (ACD/Labs, 2017).

[c] $\log_{10}$(C*) values calculated using methods outlined in Pankow, et al. (Pankow, 1994). An activity coefficient of 1.3 was assumed based on a typical estimated BBOA activity coefficient of 1.3 (Donahue et al., 2011).

[d] Defined using criteria set forth in previous work (Donahue et al., 2011, 2012).

Table S5. Raw SIC integrations, reported as a triplicate average ± one standard deviation (%), for each compound reported in Table S2 at each equivalent aging time.

Compound	Ion Integrated	Equivalent Aging Time (days)		
		0	3.4	9.8
1,6-anhydro-β-glucopyranose (levoglucosan)	60	1808457 ± 81.0%	204658 ± 105%	30721 ± 82.8%
Quinic Acid	60	11018541 ± 58.1%	1853570 ± 95.0%	563580 ± 100%
Mannose	60	1251912 ± 69.5%	50679 ± 85.7	3009 ± 72.7%
Octadecanoic Acid	60	152898 ± 84.2%	9662 ± 44.4%	0*
Tricosane (C_{23} alkane)	57	1436688 ± 40.5%	586016 ± 18.4%	333239 ± 26.7%
Pentacosane (C_{25} alkane)	57	2906372 ± 50.0%	1058663 ± 21.9%	436707 ± 35.6%
Tetracosanal (C_{24} aldehyde)	82	5677688 ± 28.5%	2827439 ± 23.9%	662488 ± 133%
Tetracosanol (C_{24} alcohol)	97	25287834 ± 40.7%	7149720 ± 52.5%	1668500 ± 91.4%
Hexacosanal (C_{26} aldehyde)	82	4848128 ± 52.5	816648 ± 51.9%	123991 ± 100%
Nonacosane (C_{29} alkane)	57	5239775 ± 47.4%	1999041 ± 22.8%	754266 ± 43.8%
Octacosanal (C_{28} aldehyde)	82	5289335 ± 60.5%	469549 ± 74.3%	37070 ± 105%
Triacontanal (C_{30} aldehyde)	82	2726165 ± 73.7%	79372 ± 76.1%	3974 ± 141%
Dotriacontanal (C_{32} aldehyde)	82	624787 ± 81.1%	0*	0*
D:A-Friedoolean-6-ene	95	1579365 ± 37.8%	625577 ± 30.1%	220015 ± 60.3%
Friedelan-3-one (Friedelin)	95	1691654 ± 53.5%	316440 ± 51.7%	73358 ± 75.3%

*Signal not present above noise in any of the triplicate chromatograms.

Table S6. Raw SIC integrations, reported as a triplicate average ± one standard deviation (%), for each compound reported in Table S3 at each equivalent aging time.

Compound	Ion Integrated	Equivalent Aging Time (days)		
		0	3.4	9.8
2,6-dimethoxy-phenol (syringol)	154	1201740 ± 10.2%	3010168 ± 5.56%	1336464 ± 4.77%
4-hydroxy-3-methoxy-benzaldehyde (vanillin)	152	507509 ± 22.5%	6109405 ± 5.27%	1377979 ± 16.5%
4-(1,2-propadienyl)-guaiacol	162	1993611 ± 12.5%	150577 ± 9.07%	20772 ± 12.1%
1,6-anhydro-β-glucopyranose (levoglucosan)	60	18902529 ± 6.04%	24208958 ± 11.0%	4198164 ± 12.5%
galacto-heptulose	60	558671 ± 27.6%	1066469 ± 21.6%	155169 ± 3.62%
1,6-anhydro-α-d-galactofuranose	60	74564 ± 10.2%	107780 ± 14.0%	0*
guanosine	60	79398 ± 7.43%	105568 ± 1.78%	21293 ± 0.491%
n-acetyl-d-galactosamine	60	152367 ± 10.9%	205321 ± 7.25%	50226 ± 5.28
2,6-di-methoxy-4-vinyl-phenol (4-vinyl-syringol)	180	987072 ± 3.72%	764852 ± 2.06	302326 ± 9.09%
4-hydroxy-3,5-dimethoxy-benzaldehyde (syringaldehyde)	182	2918961 ± 13.8%	8383320 ± 1.87%	2704184 ± 13.3%
2,6-dimethoxy-4-(1-propynyl)-phenol	192	2291745 ± 11.3%	93509 ± 10.5%	12448 ± 20.8%
1-(4-hydroxy-3,5-dimethoxyphenyl)-ethanone (acetosyringone)	181	1893305 ± 9.62%	1374845 ± 1.85%	559574 ± 9.48%
3-(4-hydroxy-3-methoxyphenyl)prop-2-enal (coniferaldehyde)	178	2229631 ± 25.8%	874140 ± 5.91%	88980 ± 23.5%
4-(2-oxopropyl)-syringol (syringyl acetone)	210	2611809 ± 13.6%	1364254 ± 6.01%	165647 ± 22.3%
4-hydroxy-2-methoxycinnamaldehyde (sinapaldehyde)	208	20025099 ± 4.07%	8043741 ± 1.18%	1467539 ± 13.1%

*Signal not present above noise in any of the triplicate chromatograms.

Table S7. Dot products of mass spectral vectors obtained from TAG chromatograms collected using two different fuel masses at each equivalent aging time. A dot product of 1 signifies a perfect mass spectral match, and a dot product of 0 indicates a complete mismatch (Stein and Scott, 1994).

Fuel Type	Equivalent Aging Time (days)		
	0	3.4	9.8
Leaf	0.847	0.764	0.787
Wood	0.934	0.784	0.843

Table S8. Relative abundances of integrated compounds displayed in Figure 20, presented as triplicate-averaged percentages of the total compound window *m/z* 60 signal.

Fuel Type	Compound	Equivalent Aging Time (days)		
		0	**3.4**	**9.8**
Leaf	levoglucosan	8.35 ± 3.61%	4.92 ± 1.69%	3.20 ± 0.0699%[a]
	quinic acid	60.7 ± 5.50%	44.5 ± 16.1%	48.8 ± 7.86%[a]
	mannose	5.00 ± 2.89%	1.43 ± 0.122%	0.341 ± 0.0831%[a]
	octadecanoic acid	0.698 ± 0.396%	0.405 ± 0.182%	0[b]
Wood	guanosine	0.348 ± 0.0344%	0.364 ± 0.0429%	0.363 ± 0.0229%
	levoglucosan	82.4 ± 1.36%	82.3 ± 0.285%	70.7 ± 1.30%
	galacto-heptulose	2.42 ± 0.590%	3.59 ± 0.369%	2.64 ± 0.0849%
	n-acetyl-d-galactosamine	0.663 ± 0.0457%	0.702 ± 0.0588%	0.851 ± 0.0248%
	1,6-anhydro-α-d-galactofuranose	0.325 ± 0.0216%	0.367 ± 0.0358%	0[b]

[a] Signal only present above noise in two of three triplicate chromatograms; values are therefore obtained using the two chromatograms with sufficient signal.
[b] Signal not present above noise in any of the triplicate chromatograms.

References.

ACD/Labs: Advanced Chemistry Development (ACD/Labs) Software V11.02 (© 1994–2012 ACD/Labs), Retrieved from http: //www.cas.org/products/scifinder, 11 May, 2017.

Davis, D. D., Ravishankara, A. R. and Fischer, S.: SO2 oxidation via the hydroxyl radical: Atmospheric fate of HSOx radicals, Geophys. Res. Lett., 6(2), 113–116, doi:10.1029/GL006i002p00113, 1979.

Donahue, N. M., Epstein, S. A., Pandis, S. N. and Robinson, A. L.: A two-dimensional volatility basis set: 1. organic-aerosol mixing thermodynamics, Atmos Chem Phys, 11(7), 3303–3318, doi:10.5194/acp-11-3303-2011, 2011.

Donahue, N. M., Kroll, J. H., Pandis, S. N. and Robinson, A. L.: A two-dimensional volatility basis set – Part 2: Diagnostics of organic-aerosol evolution, Atmos Chem Phys, 12(2), 615–634, doi:10.5194/acp-12-615-2012, 2012.

Ehhalt, D. H., Dorn, H.-P. and Poppe, D.: The chemistry of the hydroxyl radical in the troposphere, Proc. R. Soc. Edinb. Sect. B Biol. Sci., 97, 17–34, doi:10.1017/S0269727000005273, 1990.

Gulz, P. G. and Boor, G.: Seasonal Variations in Epicuticular Wax Ultrastructures of Quercus robur Leaves, Z Naturforsch, 47c, 807–814, 1992.

Kang, E., Root, M. J., Toohey, D. W. and Brune, W. H.: Introducing the concept of Potential Aerosol Mass (PAM), Atmos Chem Phys, 7(22), 5727–5744, doi:10.5194/acp-7-5727-2007, 2007.

Kreisberg, N. M., Hering, S. V., Williams, B. J., Worton, D. R. and Goldstein, A. H.: Quantification of Hourly Speciated Organic Compounds in Atmospheric Aerosols, Measured by an In-Situ Thermal Desorption Aerosol Gas Chromatograph (TAG), Aerosol Sci. Technol., 43(1), 38–52, doi:10.1080/02786820802459583, 2009.

Lambe, A. T., Ahern, A. T., Williams, L. R., Slowik, J. G., Wong, J. P. S., Abbatt, J. P. D., Brune, W. H., Ng, N. L., Wright, J. P., Croasdale, D. R., Worsnop, D. R., Davidovits, P. and Onasch, T. B.: Characterization of aerosol photooxidation flow reactors: heterogeneous oxidation, secondary organic aerosol formation and cloud condensation nuclei activity measurements, Atmos Meas Tech, 4(3), 445–461, doi:10.5194/amt-4-445-2011, 2011.

Levy, H.: Normal Atmosphere: Large Radical and Formaldehyde Concentrations Predicted, Science, 173(3992), 141–143, 1971.

Li, R., Palm, B. B., Ortega, A. M., Hlywiak, J., Hu, W., Peng, Z., Day, D. A., Knote, C., Brune, W. H., de Gouw, J. A. and Jimenez, J. L.: Modeling the Radical Chemistry in an Oxidation Flow Reactor: Radical Formation and Recycling, Sensitivities, and the OH Exposure Estimation Equation, J. Phys. Chem. A, 119(19), 4418–4432, doi:10.1021/jp509534k, 2015.

Mao, J., Ren, X., Brune, W. H., Olson, J. R., Crawford, J. H., Fried, A., Huey, L. G., Cohen, R. C., Heikes, B., Singh, H. B., Blake, D. R., Sachse, G. W., Diskin, G. S., Hall, S. R. and Shetter, R. E.: Airborne measurement of OH reactivity during INTEX-B, Atmos Chem Phys, 9(1), 163–173, doi:10.5194/acp-9-163-2009, 2009.

NIST Mass Spec Data Center, S.E. Stein, director "Mass Spectra" in NIST Chemistry WebBook, NIST Standard Reference Database Number 69, National Institute of Standards and Technology, Gaithersburg MD, 20899, retrieved 4 June, 2017.

Palm, B. B., Campuzano-Jost, P., Ortega, A. M., Day, D. A., Kaser, L., Jud, W., Karl, T., Hansel, A., Hunter, J. F., Cross, E. S., Kroll, J. H., Peng, Z., Brune, W. H. and Jimenez, J. L.: In situ secondary organic aerosol formation from ambient pine forest air using an oxidation flow reactor, Atmos Chem Phys, 16(5), 2943–2970, doi:10.5194/acp-16-2943-2016, 2016.

Pankow, J. F.: An absorption model of gas/particle partitioning of organic compounds in the atmosphere, Atmos. Environ., 28(2), 185–188, doi:10.1016/1352-2310(94)90093-0, 1994.

Peng, Z., Day, D. A., Stark, H., Li, R., Lee-Taylor, J., Palm, B. B., Brune, W. H. and Jimenez, J. L.: HOx radical chemistry in oxidation flow reactors with low-pressure mercury lamps systematically examined by modeling, Atmos Meas Tech, 8(11), 4863–4890, doi:10.5194/amt-8-4863-2015, 2015.

Peng, Z., Day, D. A., Ortega, A. M., Palm, B. B., Hu, W., Stark, H., Li, R., Tsigaridis, K., Brune, W. H. and Jimenez, J. L.: Non-OH chemistry in oxidation flow reactors for the study of atmospheric chemistry systematically examined by modeling, Atmos Chem Phys, 16(7), 4283–4305, doi:10.5194/acp-16-4283-2016, 2016.

Shetter, R. E., Cantrell, C. A., Lantz, K. O., Flocke, S. J., Orlando, J. J., Tyndall, G. S., Gilpin, T. M., Fischer, C. A., Madronich, S., Calvert, J. G. and Junkermann, W.: Actinometric and radiometric measurement and modeling of the photolysis rate coefficient of ozone to O(1D) during Mauna Loa Observatory Photochemistry Experiment 2, J. Geophys. Res. Atmospheres, 101(D9), 14631–14642, doi:10.1029/96JD00211, 1996.

Stein, S. E. and Scott, D. R.: Optimization and testing of mass spectral library search algorithms for compound identification, J. Am. Soc. Mass Spectrom., 5(9), 859–866, doi:10.1016/1044-0305(94)87009-8, 1994.

Wong, Z., Chen, K. and Li, J.: Formation of Vanillin and Syringaldehyde in an Oxygen Delignification Process, BioResources, 5(3), 1509–1516, doi:10.15376/biores.5.3.1509-1516, 2010.